Modeling of heat flow and effective thermal conductivity of fractured media: analytical and numerical methods

S.T. Nguyen[a,b,], M.-H. Vu[b], M.N. Vu[b] and A.M. Tang[c]*

(a) Euro-Engineering, Pau, France

(b) R&D Center, Duy Tan University, Da Nang, Viet Nam

(c) Université Paris-Est, Laboratoire Navier (ENPC-IFSTTAR-CNRS) 77455 Marne la Vallée, France

(*) Corresponding author: stuan.nguyen@gmail.com

Abstract

The present work aims at modeling the thermal conductivity of fractured materials using homogenization-based analytical and pattern-based numerical methods. These materials are considered as a network of cracks distributed inside a solid matrix. Heat flow through such media is perturbed by the crack system. The problem of heat flow across a single crack is firstly investigated. The classical Eshelby's solution, extended for the calculation of the conductivity of a mixture of an ellipsoidal inclusion in an infinite homogeneous matrix, gives an analytical solution of temperature discontinuity across a non-conducting penny-shape crack. This solution is then validated by the numerical simulation based on the finite elements method. The numerical simulation allows analyzing the effect of crack conductivity. The problem of a single crack is then extended to media containing multiple cracks. Analytical estimations for effective thermal conductivity, that take into account the interaction between cracks and their spatial distribution, are developed for the case of non-conducting cracks. Pattern-based numerical method is then employed for both cases non-conducting and conducting cracks. In the case of non-conducting cracks, numerical and analytical methods, both account for the spatial distribution of the cracks, fit perfectly. In the case of conducting cracks, the numerical analyzing of crack conductivity effect shows that highly conducting cracks weakly affect heat flow, and the effective thermal conductivity of fractured media.

Keywords: morphologically representative pattern; thermal conductivity; homogenization; fractured rock

1. Introduction

Thermal conductivity is an important geophysical property of rocks and largely investigated in geo-sciences such as, nuclear waste disposal, geothermal production, CO_2 storage, hydrocarbon formation processes, etc (Tang and Cui, 2009; Tang et al., 2008; Cui et al, 2011). This parameter is generally affected by natural cracks distributed in the geomaterials. The homogenization-based analytical approach has been confirmed to be a powerful tool to estimate effective properties of heterogeneous materials (Eshelby, 1957; Mori and Tanaka, 1973; Giraud et al., 2007; Zimmerman, 1989). The macroscopic mechanical properties is affected by the properties of each phase in the mixture, the shape and the orientation of the particles as well as the stress acting on the considered materials. Nguyen and colleagues successfully employed this technique for the simulation of effective viscoelastic properties of fractured media (Nguyen et al., 2011, Nguyen, 2014a; Nguyen et al., 2015c) and effective elastic properties and electrical conductivity of sandstone (Nguyen, 2014b, Nguyen et al, 2015a,b).

Besides, the numerical approach based on the pattern-based method (PBM) is also used to simulate overall properties of heterogeneous materials (Bornert, 1996; Stolz and Zaoui, 1991). This approach is more powerful than the classical numerical finite element method (FEM) that simulates the whole representative elementary volume (REV) of the medium, in term of calculation time. Actually, the PBM considers a morphologically representative pattern (MRP) of the medium instead of the REV. For the case of fractured media, MRP contains only one crack whereas REV contains a whole system of micro-cracks (Pouya et al., 2013; Camacho and Ortiz, 1996). However, by managing the boundary condition and the shape of the MRP, the pattern-based method allows accounting for the interaction between cracks and their spatial distribution (Nguyen and Dormieux, 2014).

This paper focuses on the thermal conductivity of fractured materials based on homogenization-based analytical method and PBM. The problem of heat flow through a medium containing a single crack is firstly considered. The classical Eshelby's theory, extended for the conductivity of a mixture of an ellipsoidal inclusion in an infinite homogeneous matrix, gives an analytical solution of temperature discontinuity across a non-conducting penny-shape crack. This analytical solution is then compared with the numerical simulation based on PBM. The effect of crack conductivity is also analyzed with the help of the numerical simulation. Secondly, the problem of single crack is extended to a medium containing multiple cracks. Analytical estimations of effective thermal conductivity for the case of non-conducting cracks, that accounts the interaction between the cracks and their spatial distribution, are developed. PBM is then employed for both cases, non-conducting and conducting cracks.

Notations

- $\boldsymbol{A}$ is the second order temperature field localization tensor
- $\mathbf{1}$ is the second order unit tensor
- $[T]$ is the temperature jump across a crack
- $[t]$ is the dimensionless temperature jump across a crack
- $\underline{\nabla T}$ is the temperature gradient
- $\underline{\mathrm{z}}$ is the position vector of a point
- f is the volume fraction
- C is the conductivity
- Q is the anisotropic parameters of the inclusion
- X and X_d are the aspect ratio of the cracks and of the spatial distribution of the cracks respectively

The exponents and index

- s is for the solid phase
- c is for crack

- T is for transversal component of the transversely isotropic tensors
- N is for normal component of the transversely isotropic tensors
- mt is for Mori-Tanaka scheme
- cw is for Castañeda-Willis scheme

2. Heat flow across a single crack

One considers a basic problem of a single crack in a homogenous medium under a far-field homogenous temperature gradient condition: $\forall \underline{z} \to \infty : T = \underline{\nabla T}.\underline{z}$ (see Fig. 1). Heat flow is locally perturbed around the crack due to the contrast between the conductivity of the crack and that of the surrounding solid matrix. Temperature is discontinued across the crack.

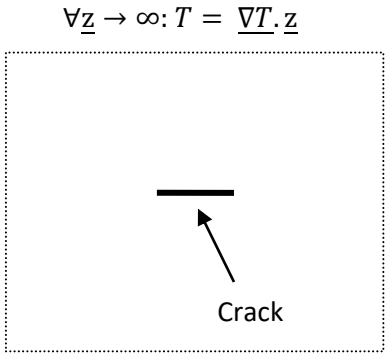


Figure1: Single crack in homogenous medium under far-field homogeneous temperature gradient boundary condition.

Note that for penny-shape crack, an extension of Eshelby's theory (Eshelby, 1957) for the problem of heat flow yields a temperature field localization tensor $\boldsymbol{A}$ that is determined by (Giraud, 2007; Nguyen, 2014):

$$\boldsymbol{A} = \frac{C_s}{(1-Q)C_s + QC_c}\left(\mathbf{1} - \underline{e_3}\otimes\underline{e_3}\right) + \frac{C_s}{2QC_s + (1-2Q)C_c}\underline{e_3}\otimes\underline{e_3} \qquad \textbf{(1)}$$

where C_s (resp. C_c) is the conductivity of the solid matrix (resp. the conductivity of the crack), $\underline{e_3}$ the unit normal to the crack plan, and Q the geometry factor defined by:

$$Q = \frac{1}{2} - \frac{\sqrt{1-X^2} - X\arctan\left(\frac{\sqrt{1-X^2}}{X}\right)}{2(1-X^2)^{3/2}} \quad \textbf{(2)}$$

98 with X is the aspect ratio of the crack (ratio between the width and the diameter of the crack,
99 see also Dormieux, 2006).Thus, for penny-shape crack we have: $X \to 0$ and

$$Q \approx \frac{\pi}{4}X \quad \textbf{(3)}$$

100 Introducing eq. (3) into eq. (1) yields:

$$\boldsymbol{A} = \frac{C_s}{(1-\frac{\pi}{4}X)C_s + \frac{\pi}{4}XC_c}\left(\mathbf{1} - \underline{e}_3 \otimes \underline{e}_3\right) + \frac{C_s}{\frac{\pi}{2}XC_s + \left(1-\frac{\pi}{2}X\right)C_c}\underline{e}_3 \otimes \underline{e}_3 \quad \textbf{(4)}$$

101 The local temperature gradient inside the crack, $\underline{\nabla T_c}$ is homogeneous and is linearly related
102 to the far-field temperature gradient (Fig. 1) as:

$$\underline{\nabla T_c} = \boldsymbol{A}.\underline{\nabla T} \quad \textbf{(5)}$$

103 Its component normal to the crack plan is expressed as:

$$\nabla T_{c,3} = \frac{C_s}{\frac{\pi}{2}XC_s + \left(1-\frac{\pi}{2}X\right)C_c}\nabla T_3 \quad \textbf{(6)}$$

104 According to this solution, the temperature jump across the crack $[T]$ is calculated as:

$$[T] = \nabla T_{c,3}d = \left(\frac{C_s}{\frac{\pi}{2}XC_s + \left(1-\frac{\pi}{2}X\right)C_c}\nabla T_3\right)d \quad \textbf{(7)}$$

105 where d is the distance between two crack's lips at the considering point. Suppose that the
106 crack has a spheroidal shape, d is calculated by:

$$d = 2X\ell\sqrt{1-\left(\frac{\rho}{\ell}\right)^2} \quad \textbf{(8)}$$

107 where ℓ and ρ are the radius of the crack and the distance to the crack's center, respectively.
108 The combination of (7) and (8) yields:

$$[T] = \left(\frac{C_s}{\frac{\pi}{2} X C_s + \left(1 - \frac{\pi}{2} X\right) C_c} \nabla T_3 \right) 2X\ell \sqrt{1 - \left(\frac{\rho}{\ell}\right)^2} \quad \textbf{(9)}$$

It is convenient to introduce also the following dimensionless temperature discontinuity:

$$[t] = \frac{[T]}{\nabla T_3} \frac{1}{\ell} = \left(\frac{2XC_s}{\frac{\pi}{2} X C_s + \left(1 - \frac{\pi}{2} X\right) C_c} \right) \sqrt{1 - \left(\frac{\rho}{\ell}\right)^2} \quad \textbf{(10)}$$

For the case of conducting crack, i.e. $C_c > 0$, the limit $X \to 0$ (penny-shape crack) yields $[t] \to 0$. More precisely, there is no temperature jump across a penny-shape conducting crack. For the case of non-conducting penny-shape crack ($C_c = 0$), equation (10) is simplified (see also Sevostianov, 2006; Vu et al., 2015) as:

$$[t] = \frac{4}{\pi} \sqrt{1 - \left(\frac{\rho}{\ell}\right)^2} \quad \textbf{(11)}$$

The maximum value of $[t] = 4/\pi$ is found at the center of the crack ($\rho = 0$). The analytical solution (11) could be considered as a reference to compare with the numerical simulation.

Considering the FEM approach for the simulation of this basic problem of heat flow across a single crack, a vertical cylinder containing a horizontal penny-shape crack is analyzed (Fig. 2). Unit vertical temperature gradient is applied on the boundary of the cylinder: $T = \underline{e}_3 . \underline{z}$. The dimension of the cylinder is chosen large enough to ensure the far-field boundary condition. The calculation is performed in axis symmetric model thank to the symmetry of the problem.

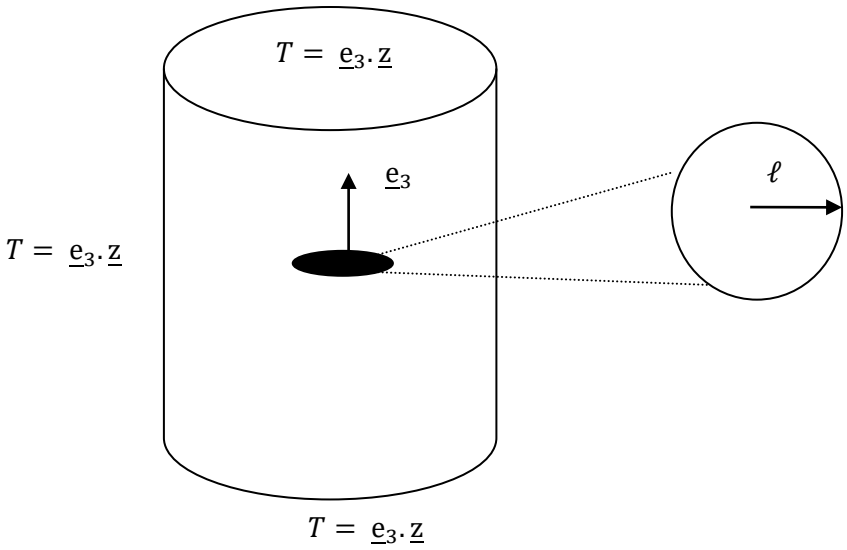


Figure 2: Numerical simulation of heat flow across a single crack: geometry and boundary conditions.

In this model, the crack is defined by a thin horizontal domain with a given conductivity. Zero conductivity is chosen for the crack's domain when modeling a non-conducting crack. The thickness of the crack domain is chosen small enough to ensure the convergence of the results. It is verified that, a ratio between the thickness and the radius of the crack smaller than 0.005 is enough. The mesh is refined around the crack, therefore a too small crack's thickness will unnecessarily raise the calculation time. The simulation is carried out by using FEM codes Cast3M (Bentejac and Hourdequin, 2005). Fig. 3 displays the mesh (in axis symmetric model), the temperature distribution in the whole domain (left side) and the local vertical temperature gradient across the crack (right side).

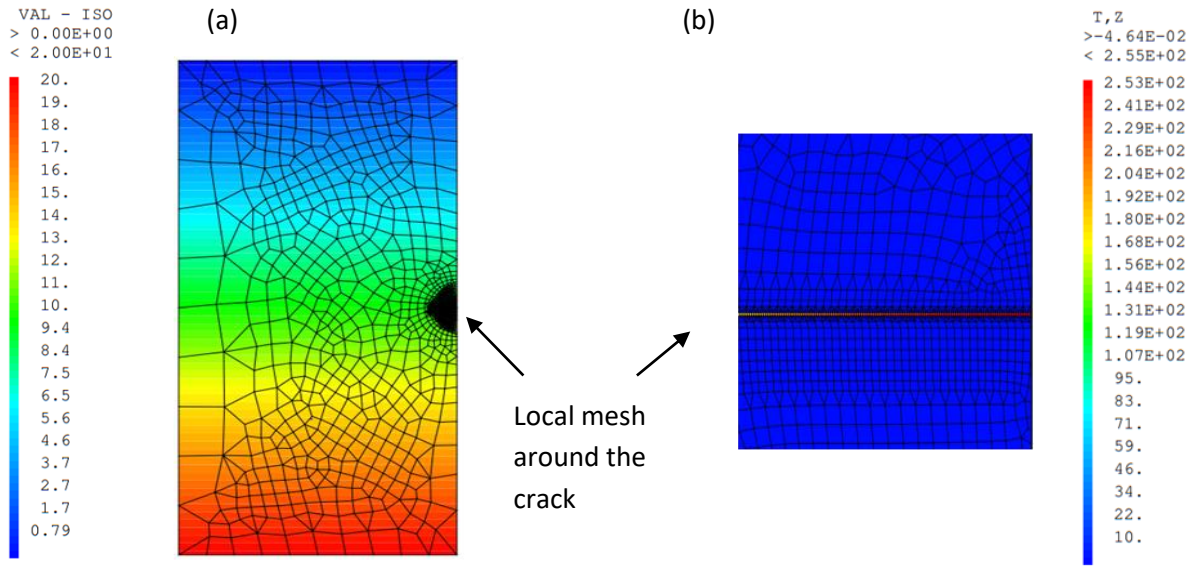


Figure 3: Numerical simulation of heat flow across a single crack: (a) temperature distribution; (b) Local temperature gradient across the crack.

In the particular case of non-conducting crack, the numerical simulation of the temperature jump across the crack is compared with the analytical solution given by the eq. (11). Fig. 4 shows the dimensionless temperature discontinuity along the crack radius. A perfect fit between the numerical and the analytical approaches can be observed.

Note that the solution given by eq. (11) is for non-conducting crack such as open and dry crack. However fluid saturated or partially saturated crack and closed crack are conducting. Fig. 4 shows also the effect of the relative conductivity of the crack and of the surrounding solid matrix on the temperature jump across the crack. For $C_c/C_s \approx 0.1$, the temperature jump is negligible. For the case of water saturated cracks in rocks (based on data given by Clauser and Huenges, 1995): $C_c/C_s = C_{water}/C_s \approx 0.1 \div 0.3$. For this case, cracks do not affect the heat flow across the crack in its normal direction.

The basic solutions developed for heat flow across a single crack will be employed and generalized in the following to simulate the effective conductivity of a domain containing multiple cracks.

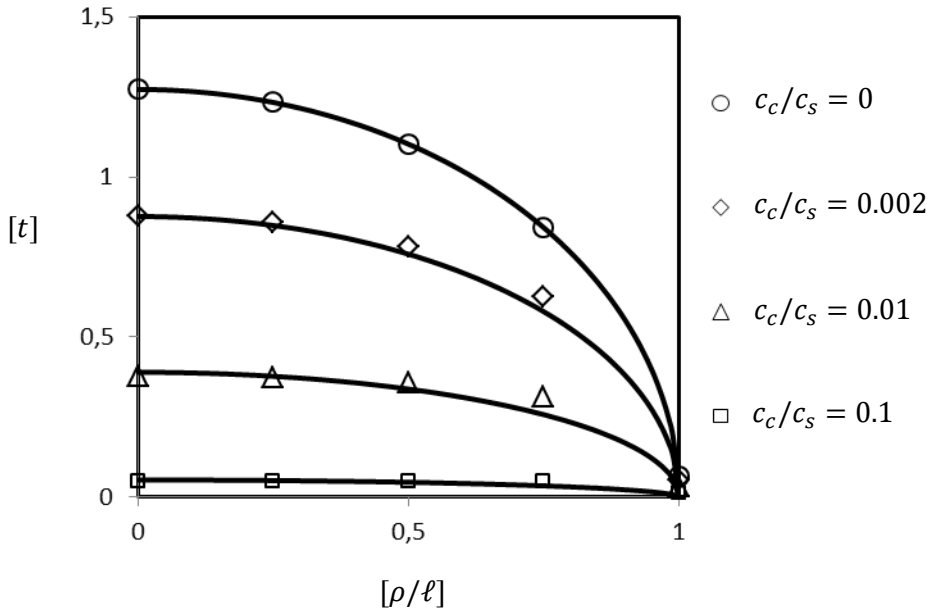


Figure 4: Temperature jump across the crack: numerical simulation (the points) and analytical result using eq. (10) (continuous line).

3. Effective thermal conductivity of cracked media

This section is dedicated to deriving the effective conductivity of media containing multiple cracks. First, the analytical homogenization-based approaches for the case of non-conducting penny-shape cracks is summarized. Second, a pattern-based numerical approach for both non-conducting and conducting cracks is developed. For non-conducting penny-shape crack, the numerical simulation is compared and constrained with the analytical estimations. The effect of crack conductivity on the effective conductivity of the whole fractured domain is considered at the end of this section.

3.1. Homogenization-based approaches

The analytical solution (11) of temperature discontinuity across a single crack is a key issue for the estimation of effective thermal conductivity for fractured media. For the case of horizontal parallel cracks in an isotropic homogeneous matrix, the effective conductivity of the medium is transversely isotropic and has on two components: conductivity in the normal

direction to the plan of the cracks ($\underline{e_3}$) and transversal conductivity. The classical Mori-Tanaka's approach, accounting the fracture interaction, gives (Mori and Tanaka, 1973; Giraud et al., 2007; Nguyen, 2014):

$$C_{mt}^N = C_s + f_c(C_c - C_s)a^N\left((1-f_c) + f_c a^N\right)^{-1}$$
$$C_{mt}^T = C_s + f_c(C_c - C_s)a^T\left((1-f_c) + f_c a^T\right)^{-1} \quad \textbf{(12)}$$

where C_{mt}^N and C_{mt}^T are the normal and transversal conductivity respectively, a^N and a^T the two corresponding components of the localization tensor defined by eq. (4)

$$a^N = \frac{C_s}{\frac{\pi}{2}XC_s + \left(1-\frac{\pi}{2}X\right)C_c};\ a^T = \frac{C_s}{(1-\frac{\pi}{4}X)C_s + \frac{\pi}{4}XC_c} \quad \textbf{(13)}$$

The volumetric fraction of the crack is defined by

$$f_c = \frac{4\pi}{3}N\delta\ell^2 = \frac{4\pi}{3}\epsilon X \quad \textbf{(14)}$$

where N is the number of cracks in a unit volume of the medium, $\delta = X\ell$ is haft of the crack's width, $\epsilon = N\ell^3$ is the crack density parameter (see also Budiansky and O'connell, 1976).

As discussed in previous section, there is no temperature jump across a penny-shape conducting crack, i.e. the penny-shape conducting cracks do not affect the effective conductivity of the medium. Considering now the case of non-conducting penny-shape cracks $C_c = 0$ and then substituting (13), (14) into (12) yields:

$$C_{mt}^N = C_s\left(1 + \frac{8}{3}\epsilon\right)^{-1};\ C_{mt}^T = C_s \quad \textbf{(15)}$$

For the case of random orientation distribution of the crack, the conductivity of the whole domain is isotropic:

$$C_{mt} = \frac{C_{mt}^N + 2C_{mt}^T}{3} = \frac{C_s}{3}\left(2 + \left(1 + \frac{8}{3}\epsilon\right)^{-1}\right) \quad \textbf{(16)}$$

The effective conductivity of fractured media can be now estimated for both parallel and random orientation distribution of cracks, by employing (15) and (16). These results account

for the interaction between the cracks but they are limited to the case of non-conducting cracks. More importantly, these solutions do not account for the spatial distribution of the cracks (see Castañeda and Willis, 1995; Bornert et al., 1996).

To take into consideration the spatial distribution of the cracks, the results obtained by Gruescu et al. (2007), an extension of the study of Castañeda and Willis (1995), for thermal conductivity C_{cw} of a system of matrix and spheroidal inclusions are considered. A spheroidal distribution of the inclusions was supposed (Fig. 5*b*).

$$C_{cw}^{N} = C_m + f_I T_I^N \left(1 - f_I T_I^N \frac{1-\frac{\pi}{2}X_d}{C_m}\right)^{-1}$$
$$C_{cw}^{T} = C_m + f_I T_I^T \left(1 - f_I T_I^T \frac{\frac{\pi}{4}X_d}{C_m}\right)^{-1} \quad \textbf{(17)}$$

with

$$T_I^N = \left(\frac{1}{C_I - C_m} + \frac{1-\frac{\pi}{2}X}{C_m}\right)^{-1} ;\ T_I^T = \left(\frac{1}{C_I - C_m} + \frac{\frac{\pi}{4}X}{C_m}\right)^{-1} \quad \textbf{(18)}$$

where C_m and C_I are the conductivity of the matrix and of the inclusions respectively, f_I is the volume fraction of the inclusions, X_d is the aspect ratio of the distribution which equal to the aspect ratio of the MRP (Fig. 6b) (Castañeda and Willis,1995). A parameter $X_d = 1$ corresponds to a spherical distribution (Fig. 5a) and a parameter $X_d \to 0$ corresponds to a aligned distribution.

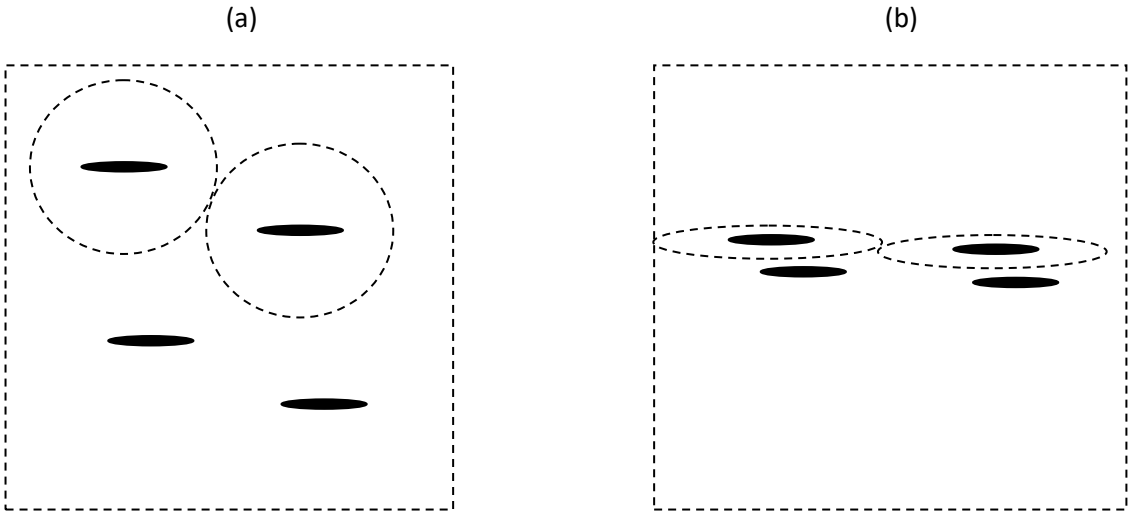


Figure 5: Spatial distribution of cracks: spherical distribution (a) and aligned distribution (b).

Applying eq. (17) for the case of inclusions are non-conducting cracks: $C_I = C_c = 0$ and $C_m = C_s$:

$$C_{wc}^N = C_s - \frac{8C_s}{3}\epsilon\left(1 + \frac{8}{3}\epsilon\left(1 - \frac{\pi}{2}X_d\right)\right)^{-1}$$
$$C_{wc}^T = C_s \quad \textbf{(19)}$$

For the case of random orientation distribution of the crack:

$$C_{cw} = \frac{C_{cw}^N + 2C_{cw}^T}{3} = C_s - \frac{8C_s}{9}\epsilon\left(1 + \frac{8}{3}\epsilon\left(1 - \frac{\pi}{2}X_d\right)\right)^{-1} \quad \textbf{(20)}$$

Note that, for the particular case of aligned distribution of the cracks (the cracks lay closely in the horizontal direction) $X_d \to 0$, (19) and (20) tend to (15) and (16):

$$\lim_{X_d \to 0} C_{wc}^N = C_s\left(1 - \frac{8}{3}\epsilon\left(1 + \frac{8}{3}\epsilon\right)^{-1}\right) = C_s\left(1 + \frac{8}{3}\epsilon\right)^{-1} \quad \textbf{(21)}$$

Analytical formulations (19) and (20) appear to be powerful to evaluate effective properties of fractured materials. However they are limited to non-conducting penny-shape cracks. In the next section, a numerical pattern-based approach will be proposed to deal with both the spatial distribution and the conductivity of the cracks.

3.2. Numerical pattern-based method

PBM is developed to simulate heat flow and effective thermal conductivity of micro-cracked media. This method considers a MRP that, as described by Bornert et al. (1996), is a sub-domain containing a single crack that represents the microstructure of the whole domain (see Fig. 6b). In the numerical simulation, an equivalent domain formed by the MRP surrounded by an infinite matrix solid is considered (Nguyen and Dormieux, 2014) (Fig. 6c). The temperature boundary condition applied on the equivalent domain is: $\forall \underline{z} \to \infty: T_o = \underline{\nabla T_o}.\underline{z}$. To account for the interaction between the cracks, the equivalent temperature gradient $\underline{\nabla T_o}$ is chosen to ensure that the average temperature of the MRP is equal to the macroscopic temperature gradient applied on the initial medium that was noted by $\underline{\nabla T}$ (see Mori and Tanaka, 1973). The numerical simulation of the equivalent problem is similar to the problem presented in the section 2. By using the FEM code Cast3M, the temperature and the heat flux field in the whole equivalent domain can be obtained.

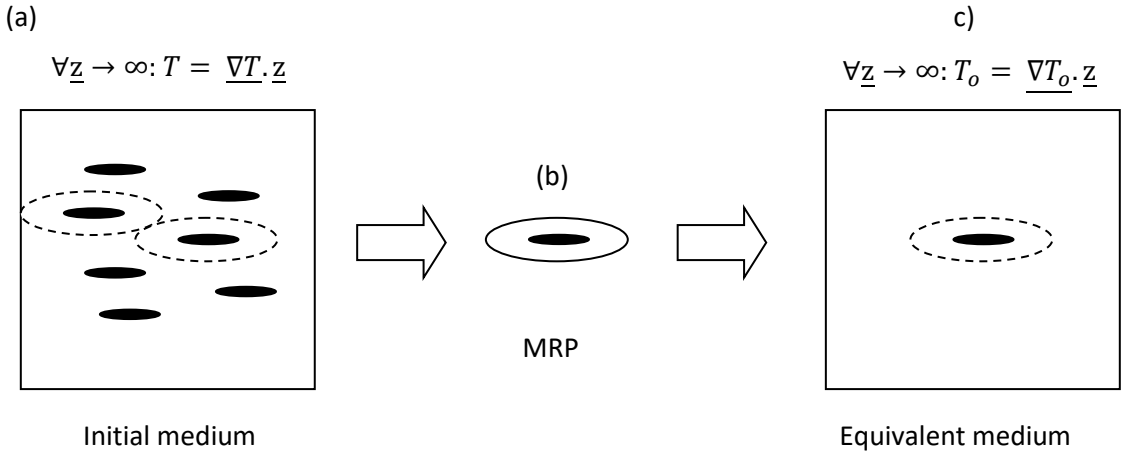


Figure 6: MRP (b) of a fractured medium (a) and its equivalent medium for numerical simulation (c).

The macroscopic heat flux is calculated by taking the average over the MRP inside the equivalent domain.

$$\underline{F} = \frac{1}{V_{MRP}} \int_{MRP} \underline{f}\, dV \tag{22}$$

Then the effective conductivity is calculated, for the case of parallel cracks, by:

$$C^N = \frac{F_3}{\nabla T_3}; C^T = C_s \tag{23}$$

and for random orientation distribution of cracks by:

$$C = \frac{C^N + 2C^T}{3} \tag{24}$$

Fig. 7 shows a comparison between the numerical simulation obtained by current method and the analytical solutions derived in previous section, for the case of parallel non-conducting cracks. A perfect fit between the numerical approach and the analytical approach (eq. (19)) can be observed. It is to note that both approaches consider the spatial distribution of the cracks. Two distribution was considered: $X_d = 0.1$ and $X_d = 0.05$. The numerical results also show that, as presented in eq. (21), when X_d tends to zero the conductivity tends to that obtained by the Mori-Tanaka method (eq. (15)).

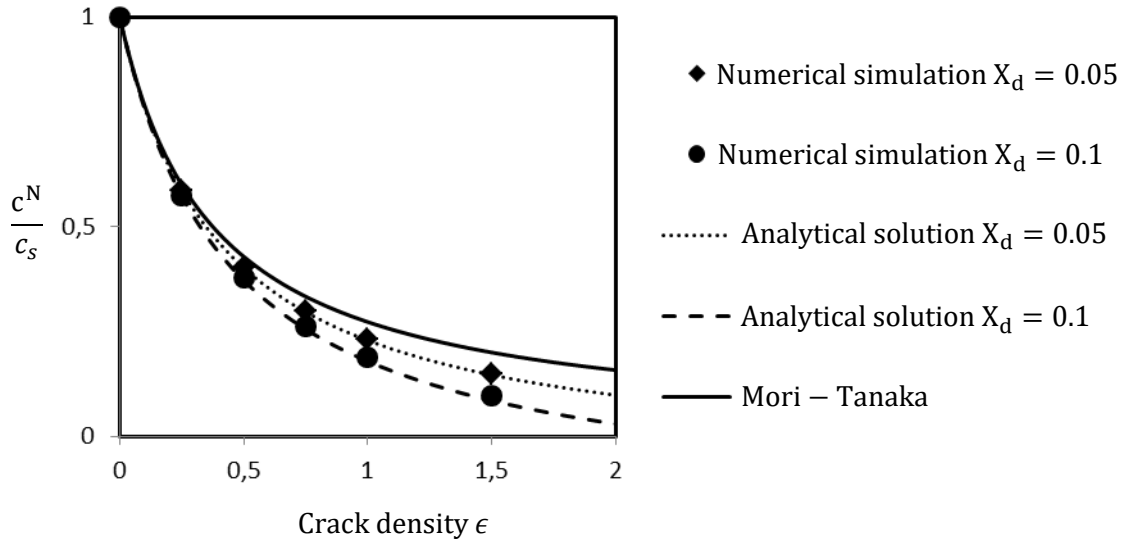


Figure 7: Comparison between the numerical PBM and the analytical homogenization-based approach.

Note that, differently from the analytical solutions, the numerical method also allows the simulation of the effective conductivity media containing conducting cracks. Fig. 8 shows the effect of the crack conductivity on the overall conductivity of the medium. The simulation suggests that, for $C_c/C_s \geq 0.1$, the effect of cracks on the overall conductivity of the fractured media is weak.

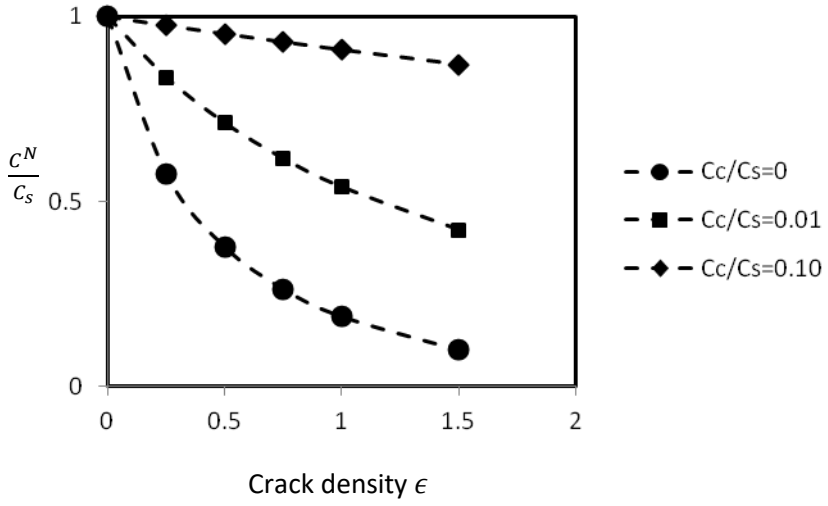


Figure 8: Effect of crack conductivity and crack density on overall conductivity of fractured media: numerical simulations.

4. **Conclusions**

Firstly, heat flow across a single crack is analyzed by both analytical and numerical methods. A closed-form solution is derived for the temperature jump across a single non-conducting crack under homogeneous gradient far-field boundary condition. This analytical formulation is then validated by the FEM simulation. The effect of crack conductivity on the temperature discontinuity is also analyzed by the numerical method. It is shown that for crack of high conductivity (for example water saturated crack), the temperature jump across the crack can be negligible and the crack affects weakly the heat flow through the whole medium.

Secondly, the basic result of heat flow across a single crack is extended for the case of multiple cracks. Homogenization-based analytical approaches and PBM are employed to

simulate effective thermal conductivity of fractured materials. Both isotropic and transversely isotropic (parallel cracks) cases are considered. The spatial distribution of the cracks is also taken into account in the analytical and numerical methods. In the particular case of non-conducting crack, the numerical and analytical methods fit perfectly together. When the distribution of the crack is aligned, both approaches tend to the analytical solution developed based on the Mori-Tanaka scheme.

The numerical PBM allows also the simulation of the effect of the crack conductivity on the overall conductivity of the fractured media. It is demonstrated that, for cracks with conductivity equal to of about 10% of the conductivity of the surrounding solid matrix (for example water saturated rocks), the effect of the cracks system on the overall conductivity of the fractured media can be negligible.

References

Tang, A. M., & Cui, Y. J. (2009). Modelling the thermo-mechanical volume change behaviour of compacted expansive clays. *arXiv preprint arXiv:0904.3614*.

Tang, A. M., Cui, Y. J., & Le, T. T. (2008). A study on the thermal conductivity of compacted bentonites. *Applied Clay Science*, *41*(3), 181-189.

Bentejac, F., & Hourdequin, N. (2005). TOUTATIS: An Application of the Cast3m Finite Element Code for PCI Three-Dimensional Modelling. In *Pellet-Clad Interaction in Water Reactor Fuels*.

Bornert, M. (1996). A generalized pattern-based self-consistent scheme. *Computational Materials Science*, *5*(1), 17-31.

Bornert, M., Stolz, C., & Zaoui, A. (1996). Morphologically representative pattern-based bounding in elasticity. *Journal of the Mechanics and Physics of Solids*, *44*(3), 307-331.

Budiansky, B., & O'connell, R. J. (1976). Elastic moduli of a cracked solid. *International Journal of Solids and Structures*, *12*(2), 81-97.

281 Camacho, G. T., & Ortiz, M. (1996). Computational modelling of impact damage in brittle
282 materials. *International Journal of solids and structures*, *33*(20), 2899-2938.
283 Castañeda, P. P., & Willis, J. R. (1995). The effect of spatial distribution on the effective
284 behavior of composite materials and cracked media. *Journal of the Mechanics and Physics*
285 *of Solids*, *43*(12), 1919-1951.
286 Clauser, C., & Huenges, E. (1995). Thermal conductivity of rocks and minerals. *Rock physics*
287 *& phase relations: A handbook of physical constants*, 105-126.
288 Cui, Y. J., Tang, A. M., Qian, L. X., Ye, W. M., & Chen, B. (2011). Thermal-mechanical
289 behavior of compacted GMZ Bentonite. *Soils and foundations*,*51*(6), 1065-1074.
290 Dormieux, L., Kondo, D., & Ulm, F. J. (2006). *Microporomechanics*. John Wiley & Sons.
291 Eshelby, J. (1957). The determination of the elastic field of an ellipsoidal inclusion and
292 related problems. *Proc. R. Soc. London,* A 241, 376–396.
293 Giraud, A., Gruescu, C., Do, D. P., Homand, F., & Kondo, D. (2007). Effective thermal
294 conductivity of tr*ansversely isotropic* media with arbitrary oriented ellipsoidal
295 inhomogeneities. *International Journal of Solids and Structures*, *44*(9), 2627-2647.
296 Gruescu, C., Giraud, A., Homand, F., Kondo, D., & Do, D. P. (2007). Effective thermal
297 conductivity of partially saturated porous rocks. *International Journal of Solids and*
298 *Structures*, *44*(3), 811-833.
299 Mori, T., & Tanaka, K. (1973). Average stress in matrix and average elastic energy of
300 materials with misfitting inclusions. *Acta metallurgica*, *21*(5), 571-574.
301 Nguyen, ST (2014a). Micromechanical approach for electrical resistivity and conductivity of
302 sandstone. *Journal of Applied Geophysics*, *111*, 135-140.
303 Nguyen, ST (2014b) Generalized Kelvin model for micro-cracked viscoelastic
304 materials. *Engineering Fracture Mechanics*, *127*, 226-234.
305 Nguyen, S. T., & Dormieux, L. (2014). Propagation of micro-cracks in viscoelastic materials:
306 Analytical and numerical methods. *International Journal of Damage Mechanics*,
307 1056789514539715.

Nguyen, ST, Dormieux, L, Le Pape, Y & Sanahuja, J (2011) A Burger model for the effective behavior of a microcracked viscoelastic solid. *International Journal of Damage Mechanics*, *20*(8), 1116-1129.

Nguyen, ST, Vu, MH, & Vu, MN (2015a). Extended analytical approach for electrical anisotropy of geomaterials. *Journal of Applied Geophysics*, *123*, 211-217.

Nguyen, S. T., Vu, M. H., & Vu, M. N. (2015b). Equivalent porous medium for modeling of the elastic and the sonic properties of sandstones. *Journal of Applied Geophysics*, *120*, 1-6.

Nguyen, TN, Nguyen, ST, Vu, MH, & Vu, MN (2015c). Effective viscoelastic properties of micro-cracked heterogeneous materials. *International Journal of Damage Mechanics*, 1056789515605557.

Pouya, A., Vu, M. N., Ghabezloo, S., & Bendjeddou, Z. (2013). Effective permeability of cracked unsaturated porous materials. *International Journal of Solids and Structures*, *50*(20), 3297-3307.

Stolz, C., & Zaoui, A. (1991). Analyse morphologique et approches variationnelles du comportement d'un milieu élastique hétérogène. *Comptes rendus de l'Académie des sciences. Série 2, Mécanique, Physique, Chimie, Sciences de l'univers, Sciences de la Terre*, *312*(3), 143-150.

Vu, M. N., Nguyen, S. T., Vu, M. H., Tang, A. M., To, V. T. (2015). Heat conduction and thermal conductivity of 3D cracked media. International Journal of Heat and Mass Transfer 89, 1119-1126.

Zimmerman, R. W. (1989). Thermal conductivity of fluid-saturated rocks. *Journal of Petroleum Science and Engineering*, *3*(3), 219-227.